Digest Journal of Nanomaterials and Biostructures Vol. 11, No. 2, April - June 2016, p. 337 - 348

ECOFRIENDLY FABRICATION OF Au/Fe_3O_4-CHITOSAN COMPOSITES FOR CATALYTIC REDUCTION OF METHYL ORANGE

X. L. LIU, X. YANG*, H. Y. XIN, X. P. TANG, L. J. WENG, Y. Y. HAN, D. GENG

Key Laboratory for Biochemical Engineering Technology of Fujian Province, College of Chemical Engineering, Huaqiao University, Xiamen, P.R. China

Au/Fe_3O_4-chitosan composites were synthesized by a green method without using any strong reducing or stabilizing agents. The morphological properties and structural features of the composites were investigated by transmission electron microscopy (TEM), X-ray diffraction patterns (XRD), thermogravimetric (TG) and Fourier transform infrared (FT-IR) techniques. Catalytic degradation of methyl orange in the presence of $NaBH_4$ using the as-prepared composite as catalysts were studied. The effects of pH value, Au content, reaction time and temperature were tested and the recycling performance of catalysts was examined. The Au/Fe_3O_4-chitosan composites showed a high catalytic activity when it was prepared with 0.5 wt% Au, pH 6.0 ± 0.1 at 50 ^oC for 1 h. The degradation rate of methyl orange followed first order kinetics. A possible degradation mechanism of methyl orange was proposed.

(Received January 27, 2016; Accepted April 5, 2016)

Keywords: Magnetic chitosan; Gold nanoparticles; Methyl orange; Catalytic degradation

1. Introduction

As Earth's population continues to grow, people are putting ever-increasing pressure on the planet's water resources. Water contamination has become a immanent problem because of the urbanization, industrialization, agriculture and mining activity of human. Among them, surface water is seriously polluted due to the discharge of sewage with toxic and refractory heavy metals or organics, which could exist in ecosystem for a long period time [1]. The increased public concern with these pollution and the stringent international environmental standards have promoted the need to develop novel treatment methods for converting them to harmless compounds. During the past two decades, noble metal nanoparticles (NPs) have attracted an enormous amount of attention in the field of wastewater treatment because of their superior physicochemical properties [2-6]. Among these noble metal NPs, Au NPs is considered to be one of the most active research object due to their unusual physical and chemical properties [7]. In addition, it is noteworthy that nanosized Au NPs have a higher Fermi potential, which leads to the lowering of reduction potential value. Therefore Au NPs can function as a versatile catalyst for many electron-transfer reactions [8], including the reduction and degradation of dyes or nitrobenzene compounds [9-12].

However from the practical point of view, immobilizing Au NPs onto inorganic solid supports, such as TiO_2, ZrO_2 and SiO_2, offers the advantage over the colloidal catalyst counterpart in easy separation and recycle of the catalyst from the reaction mixture [13-18]. It is well known that the inorganic supports usually have large surface areas, strong affinity and synergetic effects in terms of the combination of individual advantages. Importantly during the loading procedures of

* Corresponding author: yangxin@hqu.edu.cn

Au NPs, a strong reducing agent is normally essential for the reduction of Au NPs, which is distinctly contrary to the basic requirements of green chemistry [19]. Since the matrix of polymer is rich in carboxyl, hydroxyl, or amino group, it can be a useful alternative candidate for immobilization of Au NPs due to the strong complexation ability between polymer matrix and Au NPs [20, 21]. To date, Au NPs-polymer composites has been widely applied in fuel cells, sensors and catalysis [22-24]. Nevertheless, as the synthetic polymers are usually tough to be degraded naturally, it is very intriguing to look for a kind of biodegradable and biocompatible alternatives. Chitosan is regarded as an appropriate biopolymer carrier for immobilization of metal NPs because of its abundant source and excellent biocompatibility and biodegradability [25]. Furthermore chitosan can be chemically modified easily owing to its large amounts of amino and hydroxyl groups. In consequence chitosan has wide applications in biology, pharmaceutical, catalysis and water treatment [26, 27]. It can be inferred that Au NPs/chitosan composite would also be effectively applied in the corresponding industrial sector. Previous study has found that chitosan can be utilized to reduce Au ions to stable Au NPs without any strong reducing agent [28]. Unfortunately, the recovery of Au NPs/chitosan composite is not only relatively difficult using conventional separation method, but also tends to cause tremendous waste due to the existence of suspended nanoparticles in the reaction mixture.

In order to overcome the problem of separation and recycling of the catalyst, the magnetic separation technology, which has the advantages of rapid and efficient separation, is introduced into this catalytic system. Magnetic chitosan is a kind of chitosan derivatives, which not only has good mechanical properties and stability, but also has many advantages such as cost-effectiveness, and rapid recycling. In recent years, much research efforts on magnetic chitosan have been put into wastewater disposal, but most of them are based on adsorption [29-33]. Moreover magnetic nanoparticles will effectively eliminate the requirement for either solvent swelling before or catalyst filtration after the reaction [8].

In this work, we demonstrate a mild way to prepare the Au/Fe_3O_4-chitosan composite using chitosan as reducing and capping agents. Clearly the integration of magnetic separation technology with Au NPs/chitosan has many advantages, but little research has been reported so far. The synthesized nanocomposites were characterized by means of Fourier transform infrared (FTIR), X-ray diffraction patterns (XRD), thermogravimetric (TG) and transmission electron microscopy (TEM) techniques. The catalyst showed high catalytic activity and good recyclable performance in the degradative process. Moreover the catalytic degradation mechanism of methyl orange has also been presented. The as-prepared Au/Fe_3O_4-chitosan catalysts will have great potential application prospect in the catalytic degradation of dyes in wastewater.

2. Experimental

2.1 Materials

$FeCl_3 \cdot 6H_2O$, NaOH, ammonia water, glutaraldehyde and acetic acid were of analytical grade and purchased from Xilong Chemical Co. Ltd. Hydrogen tetrachloroaurate hydrate (hydrochloroauric acid·$3H_2O$), sodium borohydride ($NaBH_4$, A.R.), methyl orange (IND), $FeSO_4 \cdot 7H_2O$ (A.R.) and chitosan flakes (B.R.) were purchased from Sinopharm Chemical Reagent Co. Ltd. All solutions were prepared in deionized water prepared using a water purification system.

2.2 Synthesis of Fe_3O_4 nanoparticles

Fe_3O_4 nanoparticles were prepared by coprecipitation of Fe^{2+} and Fe^{3+} with ammonia water and treated under hydrothermal. 5.4085 g of $FeCl_3 \cdot 6H_2O$ and 2.7802 g of $FeSO_4 \cdot 7H_2O$ were dissolved in 50 mL deionized water. The mixture was transferred to a three-necked flask and heated at 70 ^oC. Then 30 % ammonia water solution was added to the stirred mixture to adjust pH value to 10.0 ± 0.1. The reaction mixture was heated for 1 h, separated by filtration, washed with distilled water and dried at 50 ^oC in vacuum oven.

2.3 Preparation of Au/Fe_3O_4-chitosan composites

0.2 g of Fe_3O_4 nanoparticles were dispersed in 50 mL chitosan solution (10 mg/mL, dissolved in 3 % acetic acid). The suspension was mixed by ultrasonic irradiation for 10 min, followed by adding 3 mL 25 % glutaraldehyde solution. 30 % ammonia water solution was subsequently added to the mixture to adjust pH value to 9.0 ± 0.1. The mixture was heated at 60 ^oC for 2 h with mechanical stirring. After washing with anhydrous ethanol and distilled water and drying, the Fe_3O_4-chitosan composites were obtained. Then 0.5 g of the as-prepared Fe_3O_4-chitosan was dispersed into $HAuCl_4$ solution. The mixture was heated at certain temperature for a certain time after adjusting the pH value, then filtered and washed with distilled water. The residue was dried at 50 ^oC in vacuum oven.

2.4 Characterization

FTIR spectra of chitosan, Fe_3O_4 nanoparticles, Fe_3O_4-chitosan composites and Au/Fe_3O_4-chitosan composites were recorded with KBr discs in the range of 4000-500 cm^{-1} on SHIMADZU FTIR-8400S. XRD patterns of the Fe_3O_4 nanoparticles, Fe_3O_4/chitosan composites and Au/Fe_3O_4-chitosan composites were obtained with Bruker D8 ADVANCE X ray diffractometer, with nickelfiltered Cu Kα radiation with 5º min^{-1} scan rate. A continuous scan mode was used to collect 2θ data from 20º to 80º. Thermogravimetric analysis were carried out for powder samples using SHIMADZU DTG-60H thermogravimetric analyzer. Sample weighing between 5 mg to 10 mg were heated from room temperature to 700 ℃. TEM images were obtained on Philips-FEI, Tecnai F30, operating at 300 kV. A small amount of sample was sonicated in 1mL ethanol for 20 min, and then the mixed slurry was added to the double side Cu grid coated with a film of carbon.

2.5 Catalytic test

The catalytic activity of the synthesized Au/Fe_3O_4-chitosan composites was evaluated towards the degradation of methyl orange in aqueous solution. 50 mL methyl orange (0.1 mM) and 50 mL $NaBH_4$ (0.04 M) were mixed in a beaker, then 0.1 g of Au/Fe_3O_4-chitosan composites were added to the solution. At regular intervals, the solution was taken 3ml for methyl orange concentration analysis. The methyl orange concentration was inspected by the absorbance of methyl orange at 464 nm with UV-vis spectra. The percentage of methyl orange degrade was calculated according to following expression:

$$\textit{Degradation}\% = \frac{A_0 - A_t}{A_0} \times 100 \quad (1)$$

Where A_0 was the initial absorbance of methyl orange and A_t was the absorbance of methyl orange after "*t*" minutes.

3. Results and Discussion

3.1 Characterizations of catalysts

3.1.1 FT-IR analysis

FTIR spectra of the Fe_3O_4 (a), chitosan (b), Fe_3O_4-chitosan composites (c) and Au/Fe_3O_4-chitosan composites (d) was shown in Fig. 1. The peak at 596.88 cm^{-1} observed in curves (a) was related to Fe-O group and the peak around 3400 cm^{-1} in curves (a-d) was related to the -OH group. The characteristic bands of saturated C-H absorption was shown at 2930.47 cm^{-1} in curves (b-d). For the naked chitosan (b), the absorption band at 1649.76 cm^{-1}, which corresponded to N-H group bending vibration. The peak of chitosan at 1395.44 cm^{-1} (-C-O- stretching of primary alcoholic group) and 1086.61 cm^{-1} (C-N bond) also appeared [34]. In the spectrum of Fe_3O_4-chitosan (c), compared with curve (b), a new peak 587.80 cm^{-1} relates to Fe-O group appeared [35]. The results suggested that the magnetic Fe_3O_4 nanoparticles succeeded in coating

with chitosan. Comparing with curve (c), the peak at 3430.04 cm^{-1} in curve (d) enhanced again suggesting that Au NPs anchored on the Fe_3O_4-chitosan layer successfully [36].

3.1.2 XRD analysis

The XRD patterns of the naked Fe_3O_4, Fe_3O_4-chitosan composites and Au/Fe_3O_4-chitosan composites were shown in Fig. 2. For Fe_3O_4 nanoparticles (a), the peaks at 2θ=30º, 36º, 43º, 54º, 57º, 63º and 74º correspond to the (211), (311), (400), (422), (511), (440) and (533), respectively [37]. After coating with chitosan, no new peaks appeared, suggesting the particles maintained the crystalline structure of Fe_3O_4 (b). When anchoring Au nanoparticles on the surface of Fe_3O_4-chitosan (c), new peaks like 38º (111), 44º (200), 65º (220), and 78º (311) appeared, which proved the successful attachment of Au nanoparticles [36].

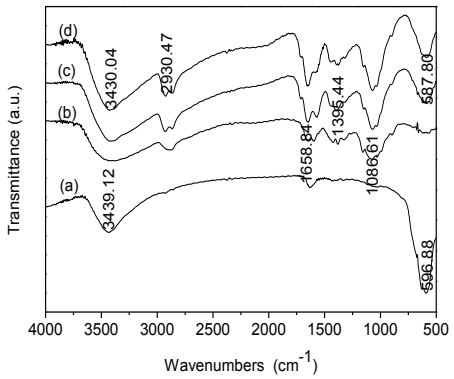

Fig. 1 FT-IR spectra of Fe_3O_4 (a), chitosan (b), Fe_3O_4-chitosan composites (c) and Au/Fe_3O_4-chitosan composites (d)

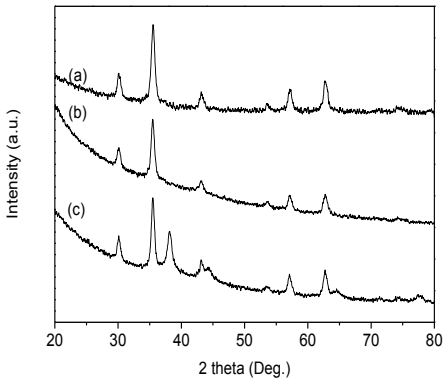

Fig. 2 XRD patterns of the naked Fe_3O_4 (a), Fe_3O_4-chitosan composites (b) and 2 wt% Au/Fe_3O_4-chitosan composites (c)

3.1.3 The thermogravimetric analysis

The thermal properties of the composites were studied by thermogravimetric analysis (TGA), and the results were shown in Fig. 3. The weight loss of the naked Fe_3O_4 nanoparticles (a) was about 4.85 % over the temperature range from 30 ^oC to 700 ^oC. There was no obvious weight loss, which might be due to the loss of moisture content in the sample [34]. From the TGA curves of chitosan (b), Fe_3O_4-chitosan composites (c) and Au/Fe_3O_4-chitosan composites (d), the weight loss observed before 200 ^oC was ascribed to the release of physically adsorbed water, while the weight losses of 44.99 %, 24.54 % and 24.41 % respectively from 250 ^oC to 400 ^oC suggested that

the chitosan began to decompose. Furthermore, 16.53 %, 34.45 % and 36.11 % weight losses appeared in chitosan, Fe_3O_4-chitosan composites and Au/Fe_3O_4-chitosan composites when the temperature increased from 400 ^oC to 700 ^oC, which might be arise from slow degradation of residual chitosan [37]. The weight loss of Au/Fe_3O_4-chitosan composites was lower than Fe_3O_4-chitosan composites because of the introduction of the Au nanoparticles.

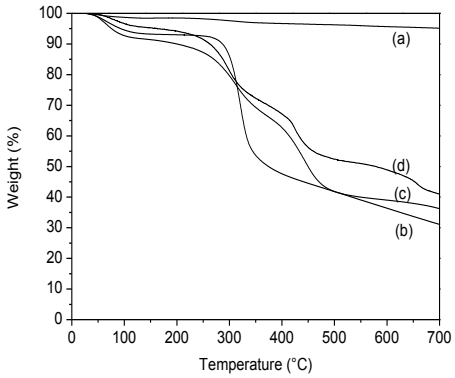

Fig. 3 Thermogravimetric analysis (TGA) of Fe_3O_4 (a), chitosan (b), Fe_3O_4-chitosan composites (c) and Au/Fe_3O_4-chitosan composites (d)

3.1.4 TEM analysis

Fig. 4 showed TEM images of Fe_3O_4-chitosan composites (a) and Au/Fe_3O_4-chitosan composites (b) catalysts. It was observed in Fig. 4(a) that the Fe_3O_4 nanoparticles could be well dispersed in chitosan without occurrence of agglomeration, which was beneficial to the magnetic properties of the magnetic chitosan carrier [38]. The comparison of Fig. 4(a) and (b) shown that the morphology of magnetic chitosan remained unchanged through the hydrothermal process for reducing $HAuCl_4$. In Fig. 4(b), some points in the diameter of less than 10 nm could be deduced as Au NPs, which indicated that Au NPs were successfully loaded on the surface of chitosan. The TEM analyses suggested that Fe_3O_4 NPs and Au NPs had good dispersion in the nanocomposites and the diameter of Fe_3O_4 NPs varied from 10 to 30 nm, while the diameter of Au NPs was less than 10 nm.

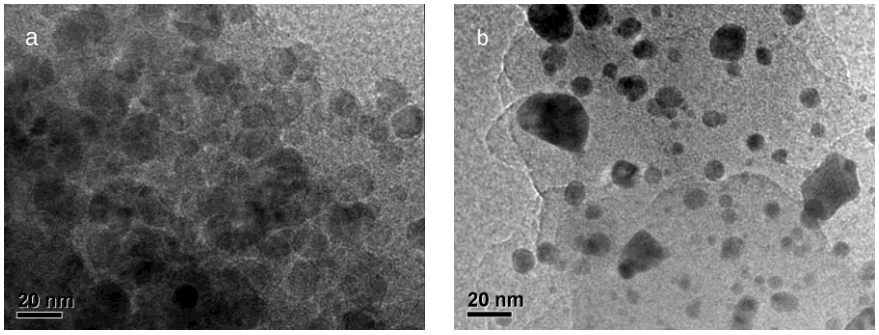

Fig. 4 TEM images of Fe_3O_4-chitosan composites (a) and Au/ Fe_3O_4-chitosan composites (b).

3.2 Catalytic activity

3.2.1 Preliminary experiment

The catalytic activity of Au/Fe_3O_4-chitosan composites were tested for the degradation of methyl orange as compared to without catalyst and using Fe_3O_4-chitosan as the catalyst. The Fig. 5 showed the fast degradation of methyl orange with time in the presence of 0.5 wt% Au/Fe_3O_4-chitosan as compared to very slow degradation for uncatalyzed reaction. However, Fe_3O_4-chitosan seemed to exhibit a maximum of 32 % of methyl orange degradation within 24 min and no significant change was observed after that, indicating certain adsorption capacity of the Fe_3O_4-chitosan.

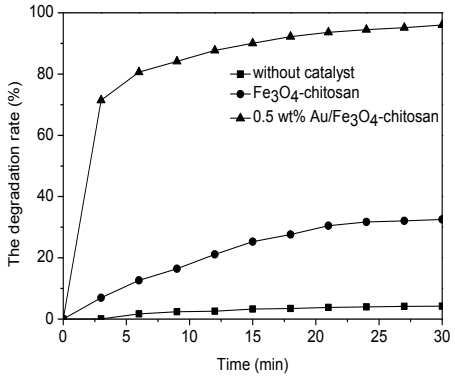

Fig. 5 Result of the degradation of methyl orange at 464 nm in uncatalyzed reaction, Fe_3O_4-chitosan catalyzed and Au/Fe_3O_4-chitosan catalyzed reaction

UV-vis absorption spectra was shown in Fig. 6. The result showed that the absorption peak of the methyl orange at 464 nm began to decline, and disappeared within 30 min. Meanwhile, the absorption peak at 272 nm occured blue shift, and the intensity increased gradually. In the end, a new absorption peak was appeared at 247 nm. This indicated that azo group of the methyl orange ruptured, and generated N,N-dimethyl aniline and sodium sulfanilate [39, 40].

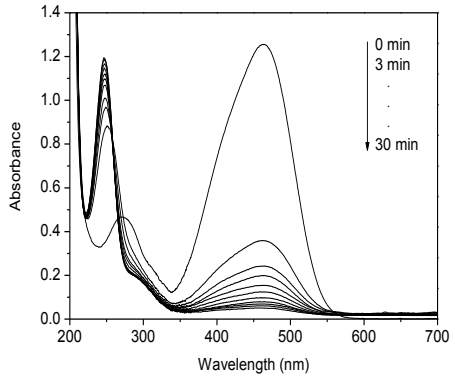

Fig. 6 UV-vis spectra of methyl orange degraded by $NaBH_4$ in presence of Au/Fe_3O_4-chitosan composites

3.2.2 Effect of Au content

The reduction of the methyl orange over Au/Fe_3O_4-chitosan with varying loading amounts was revealed in Fig. 7. The Au/Fe_3O_4-chitosan with 0.5 wt% loading showed the highest

degradation percentage among all the samples. It was found that the catalytic efficiency had hardly any change with increasing Au NPs loading amounts from 0.5 wt% to 1.5 wt%, while the catalytic efficiency over 2.0 wt% Au/Fe_3O_4-chitosan decreased slightly. The small sized Au nanoparticles possessed a higher redox potential value, which was beneficial for accelerating the electron transfer between the methyl orange and $NaBH_4$. Oppositely, the higher Au loading would block the mass transfer of the methyl orange into the inside of Fe_3O_4-chitosan to approach the catalytic sites [41].

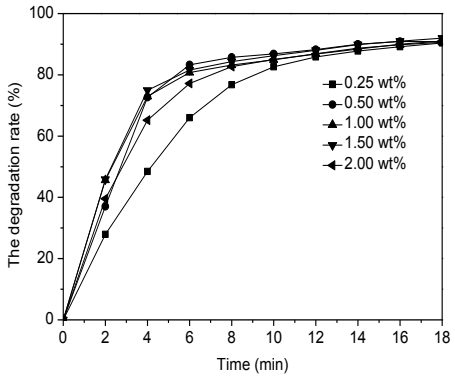

Fig. 7 Effect of Au content on the degradation of methyl orange

3.2.3 Effect of synthesis time

The synthesis time of Au/Fe_3O_4-chitosan in the range of 30 min-3 h was investigated in Fig. 8. The figure indicated that the best synthesis time was 1 h. For the longer synthesis time of 2 h, Au NPs tended to assemble into large aggregates and the catalytic activity would decrease accordingly. When synthesis time was less than 1 hour, the degradation rate of methyl orange would slow down probably due to incomplete reduction of gold ions. Therefore, 1 h was selected as a suitable synthesis time.

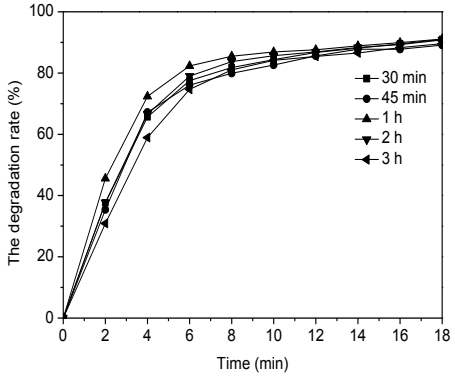

Fig. 8 Effect of synthesis time on the degradation of methyl orange

3.2.4 Effect of pH value

The results of pH values on the degradation of methyl orange were shown in Fig. 9. The result demonstrated that the methyl orange degradation rate gradually slowed down with the elevation of the pH and the fastest degradation rate was achieved at pH 6.0 ± 0.1. It was found that

the formation of Au/Fe_3O_4-chitosan composites needed two steps, namely the absorption of gold ions on Fe_3O_4-chitosan composites and the reduction of adsorbate to Au NPs by chitosan [42]. The reduction reactions of gold species were carried out smoothly at pH 6.0 ± 0.1 due to unfavorable hydrolyzation of $AuCl_4^{-1}$ by increasing hydroxide ion concentration. Distinctly the suitable pH value would guarantee the formation of Au/Fe_3O_4-chitosan composites.

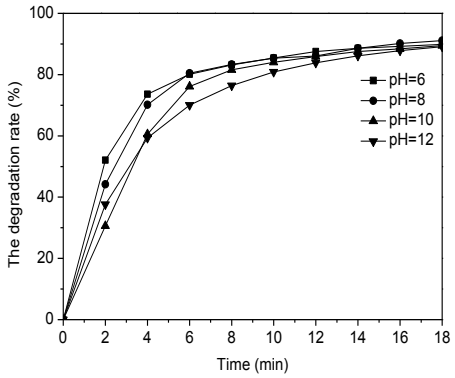

Fig. 9 Effect of pH value on the degradation of methyl orange

3.2.5 Effect of synthesis temperature

The effect of synthesis temperature on the degradation of methyl orange was shown in Fig. 10. It was found that Au/Fe_3O_4-chitosan composites prepared at 50 ^oC exhibiting the highest activity, whereas with increasing temperature continually, the degradation rate of methyl orange gradually decreased. It was worth mentioning that the higher synthesis temperature could lead to aggregation of Au NPs because of the fast nucleation and growth. Moreover, some large spheres and triangles were appearing in the nanoparticles at 80 ^oC [42]. According, selecting comparatively lower synthesis temperature such as 50 ^oC would promote the growth of Au nanoparticles.

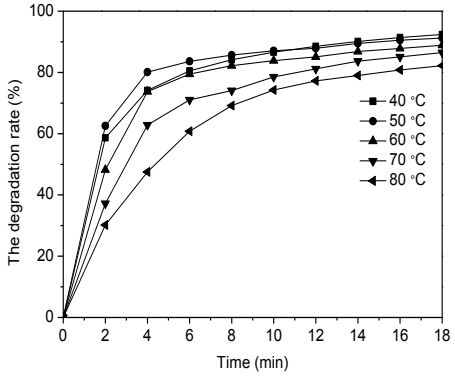

Fig. 10 Effect of synthesis temperature on the degradation of methyl orange

3.2.6 Recovery evaluation

In order to study the stability of 0.5 wt% Au/Fe_3O_4-chitosan catalyst, recycling experiments were executed. The catalysts were recycled by the application of an external magnetic field and washed with deionized water. As shown in Fig. 11, the degradation rate was nearly unchanged after twelve cycles, which indicated that the catalyst had high stability and was uneasy

to lose activity or poisoning in the system. Also, the catalyst could be completely recovered. Thus, the Au/Fe_3O_4-chitosan catalyst developed in this work exhibited excellent catalytic performance.

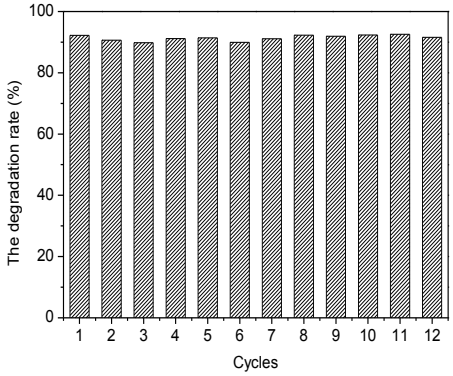

Fig. 11 Result of recycling studies. $[MO]_0$=0.1 mM, [catalyst]=2 g/L, reaction time=18 min

3.3 Kinetic and mechanism of catalytic degradation of methyl orange

In order to investigate the kinetic rate constants, C_t/C_0 and $\ln(C_t/C_0)$ *versus* reaction time for the degradation of methyl orange over different amounts of catalyst were plotted in Fig. 12. The plots of $\ln(C_t/C_0)$ *versus* reaction time yielded good linear correlations as indicated in Fig. 12(b). As shown in Table 1, the kinetic constants were 0.08366, 0.14184 and 0.28204 min^{-1} corresponding to 25, 50 and 100 mg catalyst dosage, respectively. The results indicated that the degradation of methyl orange by Au/Fe_3O_4-chitosan catalyst was consistent with the pseudo first order kinetics and the catalytic efficiency increased gradually with increasing the amount of catalyst.

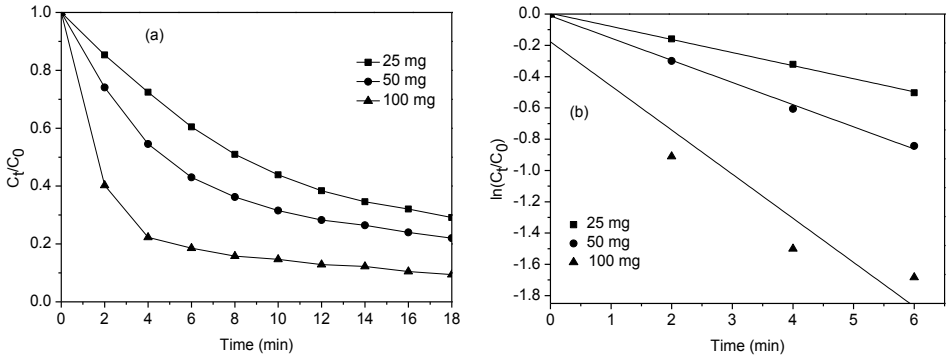

Fig. 12 (a) C_t/C_0 and (b) $ln(C_t/C_0)$ versus reaction time for the degradation of methyl orange at different amounts of catalyst

In order to study the effect of the concentration of methyl orange on the kinetic rate constants, 0.1 mg catalyst was used for 0.05, 0.10, 0.15, 0.20, 0.25 mM methyl orange. As confirmed in Fig. 13 and Table 1, the kinetic constants showed not significant changes during increase initial concentrations of methyl orange. The result of the study indicated that the catalytic efficiency was not subject to the initial methyl orange concentration.

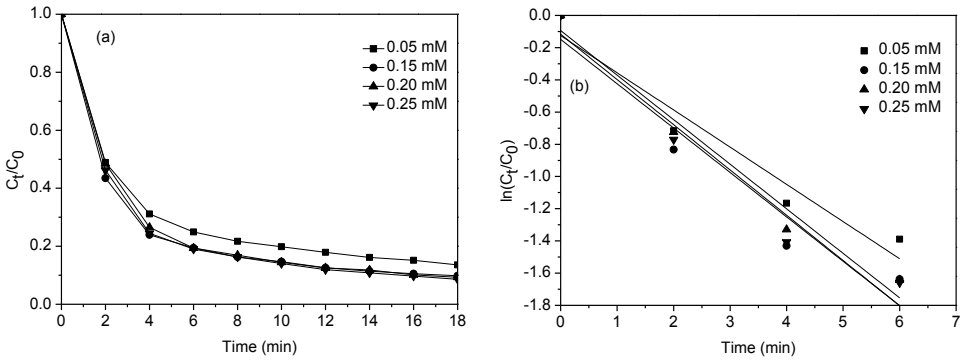

Fig. 13 (a) C_t/C_0 and (b) $\ln(C_t/C_0)$ versus reaction time for the degradation of methyl orange at different initial concentrations of methyl orange

Table 1 Comparison of various conditions for the degradation of methyl orange

Concentration of methyl orange (mM)	Catalyst usage amounts (mg)	k (min^{-1})	R^2
0.10	25	0.08366	0.99855
0.10	50	0.14184	0.99519
0.10	100	0.28204	0.88458
0.05	100	0.23095	0.91919
0.15	100	0.27558	0.90842
0.20	100	0.27658	0.95840
0.25	100	0.28084	0.93619

The plausible mechanism for the reduction of methyl orange was shown in Fig. 14. In the process of catalytic reaction, Au NPs were acted as the medium of electron transfer. In the first place, BH_4^{-1} and methyl orange quickly spread to the surface of Au nanoparticles. Afterwards, the Au NPs accepted electrons from BH_4^{-1} and passed them on to the methyl orange. Meanwhile, BH_4^{-1} was oxidized to BO_3^{3-} and the methyl orange was reduced to the corresponding aromatic amine compounds [40, 43]. The Au NPs possibly play an electron transfer role in the whole catalytic process. The following reactions (Equation 2 and 3) displayed the catalytic process in detail:

$$BH_4^- + 3H_2O \longrightarrow BO_3^{3-} + 8e^- + 10H^+ \quad (2)$$

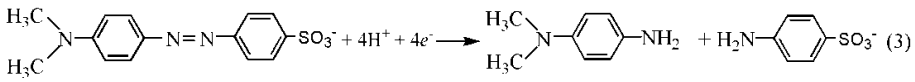

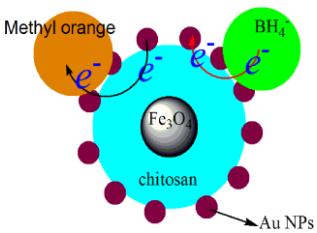

Fig. 14 The flow chart of feasible mechanism of methyl orange degradation on Au/Fe_3O_4-chitosan at the presence of $NaBH_4$

4. Conclusions

An environmentally benign method was developed to fabricate Au/Fe_3O_4-chitosan composites by combination of magnetic separation techniques with the loading of Au NPs on chitosan. The characterization results of FTIR, XRD, TG and TEM indicated that Au NPs and Fe_3O_4 NPs were discovered to be dispersed on the surface of the chitosan successfully, and Au NPs and Fe_3O_4 NPs were found to be in spherical shape with the diameter of less than 10 nm and 10~30 nm, respectively. High catalytic ability of Au/Fe_3O_4-chitosan was achieved at appropriate Au content, time, pH and temperature conditions for the degradation of methyl orange. It is worth noting that the catalysts remained stable over 12 reaction cycles with little disruption in productivity. This work appears to be useful in developing new process for the degradation of dyes in wastewater under mild condition, and will be also helpful for the development and applications of magnetically recoverable Au nanocatalysts.

Acknowledgments

We gratefully acknowledge the financial supports from the Natural Science Foundation of Fujian Province (No. 2012J05025) and the Research Foundation of Education Bureau of Fujian Province, China (JA15022).

References

[1] A. Ayati, A. Ahmadpour, F. F. Bamoharram, B. Tanhaei, M. Mänttäri, M. Sillanpää, Chemosphere, **107**, 163 (2014).
[2] Y. Mei, Y. Lu, F. Polzer, M. Ballauff, M. Drechsler, Chem. Mater. **19**, 1062 (2007).
[3] K. Jiang, H. X. Zhang, Y. Y. Yang, R. Mothes, H. Lang, W. B. Cai, Chem. Commun. **47**, 11924 (2011).
[4] R. Patel, S. Suresh, J. Hazard. Mater. **137**, 1729 (2006).
[5] S. Gupta, C. Giordano, M. Gradzielski, S. K. Mehta, J. Colloid Interface Sci. **411**, 173 (2013).
[6] N. Gupta, H. P. Singh, R. K. Sharma, J. Mol. Catal. A: Chem. **335**, 248 (2011).
[7] G. Shore, W. J. Yoo, C. J. Li, M. G. Organ, Chem. Eur. J. **16**, 126 (2010).
[8] Y. C. Chang, D. H. Chen, J. Hazard. Mater. **165**, 664 (2009).
[9] M. Rashid, T. K. Mandal, Adv. Funct. Mater. **18**, 2261 (2008).
[10] W. Wang, F. Wang, Y. Kang, A. Wang, Chem. Eng. J. **237**, 336 (2014).
[11] T. Zeng, X. Zhang, S. Wang, Y. Ma, H. Niu, Y. Cai, J. Mater. Chem. A, **1**, 11641 (2013).
[12] J. Zhang, G. Chen, M. Chaker, F. Rosei, D. Ma, Appl. Catal. B: Environ. **132**, 107 (2013).
[13] Y. Min, M. Akbulut, K. Kristiansen, Y. Golan, J. Israelachvili, Nat. Mater. **7**, 527 (2008).
[14] I. N. Remediakis, N. Lopez, J. K. Nørskov, Angew. Chem. **117**, 1858 (2005).
[15] S. S. Kim, Y. R. Kim, T. D. Chung, B. H. Sohn, Adv. Funct. Mater. **24**, 2764 (2014).
[16] Y. Wang, S. Van de Vyver, K. K. Sharma, Y. Román-Leshkov, Green Chem. **16**, 719 (2014).
[17] M. Stratakis, H. Garcia, Chem. Rev. **112**, 4469 (2012).
[18] M. Alhumaimess, Z. Lin, Q. He, L. Lu, N. Dimitratos, N. F. Dummer, M. Conte, S. H. Taylor,

J. K. Bartley, C. J. Kiely, G. J. Hutchings, Chem. Eur. J. **20**, 1701 (2014).
[19] K. Sneha, M. Sathishkuma, S. Y. Lee, M. A. Bae, Y. S. Yun, J. Nanosci. Nanotechno. **11**, 1811 (2011).
[20] Y. Shin, I. T. Bae, B. W. Arey, G. J. Exarhos, J. Phys. Chem. C, **112**, 4844 (2008).
[21] T. F. Jaramillo, S. H. Baeck, B. R. Cuenya, E. W. McFarland, J. Am. Chem. Soc. **125**, 7148 (2003).
[22] C. Yuan, W. Luo, L. Zhong, H. Deng, J. Liu, Y. Xu, L. Dai, Angew. Chem. Int. Ed. **50**, 3515 (2011).
[23] B. Li, C. Y. Li, J. Am. Chem. Soc. **129**, 12 (2007).
[24] T. K. Sarma, D. Chowdhury, A. Paul, A. Chattopadhyay, Chem. Commun. **10**, 1048 (2002).
[25] C. K. S. Pillai, W. Paul, C. P. Sharma, Prog. Polym. Sci. **34**, 641 (2009).
[26] L. Shi, X. Fang, L. Xing, M. Chen, D. Zhu, X. Guo, L. Zhao, Z. Tang, J. Chem. Soc. Pak. **33**, 929 (2011).
[27] A. Domard, Carbohydr. Polym. **84**, 696 (2011).
[28] C. Sun, R. Qu, H. Chen, C. Ji, C. Wang, Y. Sun, B. Wang, Carbohydr. Res. **343**, 2595 (2008).
[29] S. Linley, T. Leshuk, F. X. Gu, Clean-Soil Air Water, **41**, 1152 (2013).
[30] S. H. Huang, D. H. Chen, J. Hazard. Mater. **163**, 174 (2009).
[31] K. Barquist, S. C. Larsen, Microporous Mesoporous Mater. **130**, 197 (2010).
[32] G. Zhang, J. Qu, H. Liu, A. T. Cooper, R. Wu, Chemosphere, **68**, 1058 (2007).
[33] L. C. A. Oliveira, D. I. Petkowicz, A. Smaniotto, S. B. C. Pergher, Water Res. **38**, 3699 (2004).
[39] Z. Zhou, F. Jian, T. C. Lee, T. Yue, J. Alloys Compd. **581**, 843 (2013).
[40] G. Y. Li, Y. R. Jiang, K. L. Huang, P. Ding, J. Chen, J. Alloys Compd. **466**, 451 (2008).
[41] J. Hu, Y. L. Dong, Z. Rahman, Y. H. Ma, C. L. Ren, X. G. Chen, Chem. Eng. J. **254**, 514 (2014).
[42] L. Zang, J. Qiu, X. Wu, W. Zhang, E. Sakai, Y. Wei, Ind. Eng. Chem. Res. **53**, 3448 (2014).
[43] W. Zhang, S. Jia, Q. Wu, S. Wu, J. Ran, Y. Liu, J. Hou, Mater. Sci. Eng., C, **32**, 381 (2012).
[44] A. Sakalis, D. Ansorgová, M. Holčapek, P. Jandera, A. Voulgaropoulos, Int. J. Environ. Anal. Chem. **84**, 875 (2004).
[45] S. Nam, P. G. Tratnyek, Water Res. **34**, 1837 (2000).
[46] Y. Qiu, Z. Ma, P. A. Hu, J. Mater. Chem. A, **2**, 13471 (2014).
[47] D. Wei, Y. Ye, X. Jia, C. Yuan, W. Qian, Carbohydr. Res. **345**, 74 (2010).
[48] U. P. Azad, V. Ganesan, M. Pal, J. Nanopart. Res. **13**, 3951 (2011).